Design and synthesis of metal-based chemotherapeutic agents for targeted DNA interactions or DNA repair pathway modulation

Griend, C.J. van de

Chapter 5

Dual photoactivation of ruthenium-caged inhibitors

Corjan van de Griend, Maxime A. Siegler, Remus T. Dame, Sylvestre Bonnet.

Abstract

Synthetic lethality is based upon the exploitation of a genetic mutation in a tumor, where disruption of one gene does not impact cell viability but disruption of two results in cell death. Here we developed a preparative route to bind two different inhibitors to a single ruthenium photocage, thus affording a prodrug that can release two inhibitors by local photoactivation. In principle, the photorelease of two different inhibitors simultaneously at the same location could achieve synthetic lethality without a need for genetic mutations, while tumor selectivity would rely on local photoactivation. Bis-photocaged compounds $[Ru(H_2bapbpy)(X)(Y)]^{2+}$ were prepared, defined by the central tetrapyridyl ligand H_2bapbpy = 6,6'-bis(2"-aminopyridyl)-2,2'-bipyridine, and two identical or different inhibitors X and Y axially coordinated to the metal. In [**1**]Cl$_2$–[**3**]Cl$_2$ X=Y=BO2, BOCl, or BORef, a series of RAD51 inhibitors with different inhibition properties. In [**6**]Cl$_2$ and [**7**]Cl$_2$, X=BOCl and Y=STF31 or PIK75, respectively, which are a NAMPT and DNA-PK inhibitor. The control compound [**4**]Cl$_2$ with X=Y=pyridine was also prepared. All photocaged compounds remained substitutionally inert in the dark but were activated by visible light irradiation, releasing both inhibitors with photosubstitution quantum yields of ~0.06 for the first substitution and ~0.003 for the second substitution. These results demonstrate the possibility of delivering two distinct inhibitors from one single molecular prodrug released by light activation. These results pave the way towards light-triggered synthetic lethality without the requirement of a genetic mutation.

5.1 Introduction

Synthetic lethality was first observed more than a century ago, in 1922.[1] The term was coined two decades later. It describes cases where the simultaneous inactivation of two genes results in cellular death while the perturbation of a single gene does not.[2,3] The term garnered widespread attraction since the discovery of the synthetic lethal interaction of poly(ADP-ribose) polymerase (PARP) with cancers mutated in the BRCA1 and BRCA2 genes. To date, four PARP inhibitors are FDA approved, namely Olaparib, Niraparib, Rucaparib, and Talazoparib.[4–6] PARP proteins are crucial for the single-stranded break repair pathway, an important part of the DNA damage repair arsenal. Upon PARP inhibition, single-strand breaks generate double-strand breaks (DSBs) through stalled and collapsed replication forks.[7,8] While the formed DSBs can be repaired by the high-fidelity Homologous Recombination (HR) repair pathway in normal cells, BRCA mutated tumors are HR impaired. This leads to the accumulation of DSBs in the tumor but not in healthy cells, leading to selective tumor death.[9] Despite the clinical success of PARP inhibitors, synthetic lethality itself is limited by the low number of robust synthetic lethal targets currently identified, as many potential targets are not robust enough to cover the extensive genetic heterogeneity seen in tumors.[10,11]

One therapeutic opportunity that is independent from a specific gene mutation

in cancers, would be to combine the impairment of two DNA repair pathways. In triple-negative breast cancer (TNBC), the combined treatment with PARP inhibitor Veliparib and RAD51 inhibitor B02 decreased IC_{50} significantly below that of each individual inhibitor.[12] Furthermore, down-regulation of RAD51 sensitized TNBC to PARP inhibitors.[13] RAD51 is a key protein during HR and high expression of RAD51 has been correlated to poor prognosis.[14] RAD51 depletion enhanced the cytotoxicity of DNA-dependent protein kinase (DNA-PK) inhibitor KU-57788.[12] DNA-PK is crucial for DSB repair by non-homologous end joining (NHEJ). Its inhibition combined with RAD51 depletion blocks the cell's ability to repair DSBs. Although promising, combination treatments like these are limited by the loss of cancer selectivity due to the lack of an exploitable genetic mutation. However, if selectivity is achieved through an alternative approach such as light activation, combining two inhibitors could offer an optimal treatment strategy through synergy, enforcing cancer selectivity through localized light irradiation. Furthermore, the spatiotemporal control offered by light activation ensures that the two coordinated inhibitors have the same pharmacokinetics, a feat impossible for two separately administered inhibitors.

Ruthenium-based photocages with two different coordination sites in their coordination sphere offer an excellent opportunity to attach two different inhibitors to the same prodrug. In the dark, the ruthenium prodrug remains inert, thus preventing both inhibitors from doing their work; upon local light activation, however, the two inhibitors are uncaged by photosubstitution, thus generating localized cytotoxicity by the combined inhibition of the two protein targets within the same cell. In the previous chapter, we discussed the photocaging of RAD51 inhibitors based on the B02 scaffold. Here, we combine the same B02-based inhibitor with two other inhibitors, STF31 and PIK71. STF31 is a nicotinamide phosphoribosyltransferase (NAMPT) inhibitor, a key enzyme in the NAD^+ salvage pathway that is highly expressed in several cancers.[15] Defective DNA repair mechanisms have been reported to sensitize tumors towards NAMPT inhibition.[16] Furthermore, NAMPT depletion led to defective NHEJ-mediated DSB repair and enhanced HR-mediated repair reliance, potentiating NAMPT inhibition as an interesting target for combination treatment with RAD51 inhibition.[17] PIK-75 is a reversible DNA-dependent protein kinase (DNA-PK) and p110α-selective inhibitor.[18] Treatment with the inhibitor induced increased levels of H2AX phosphorylation, a commonly used hallmark for DSB formation.[19] Furthermore, DNA-PK inhibition sensitized cells to radiation- and doxorubicin-induced DNA damage.[20]

In this work, we describe the synthesis and photochemical characterization of 7 novel ruthenium-based photoactivated chemotherapy compounds characterized by two identical or different inhibitors X and Y, coordinated in a monodentate fashion to ruthenium(II) via a nitrogen atom. The formula of the compounds is [Ru(H$_2$bapbpy)(X)(Y)]$^{2+}$, where H$_2$bapbpy = 6,6'-bis(2''-aminopyridyl)-2,2'-bipyridine and X and Y are the inhibitors. Symmetric compounds [**1**]Cl$_2$ –[**3**]Cl$_2$ were prepared where X=Y=B0Cl, B02,

or B0Ref, belong to a series of RAD51 inhibitors with excellent, good, and low RAD51 inhibition properties, respectively. The bis-pyridine compound [**4**]Cl$_2$ (X=Y=C$_5$H$_5$N) serves as negative control deprived of RAD51 inhibition properties. And finally compounds [**6**]Cl$_2$ and [**7**]Cl$_2$ are dissymmetric compounds with different inhibitors in axial positions (X ≠ Y): X=B0Cl and Y=STF31 for [**6**]Cl$_2$, and X=B0Cl and Y=PIK75 for [**7**]Cl$_2$.

5.2 Synthesis and crystal structures

The synthesis of ruthenium compounds [**1**]Cl$_2$–[**4**]Cl$_2$ was achieved by straightforward one-pot reactions in acetone containing dichloro(p-cymene)ruthenium(II) dimer, H$_2$bapbpy (2.2 eq.), AgPF$_6$ (5 eq.) and the corresponding inhibitor (for [**1**]$^{2+}$–[**3**]$^{2+}$, 5 eq.) or pyridine (for [**4**]$^{2+}$), to afford first the hexafluorophosphate salts (figure 1). To increase water solubility, chloride salt metatheses afforded complexes [**1**]Cl$_2$–[**4**]Cl$_2$ in 30-54% yield. The coordination of a single equivalent of inhibitor B0Cl afforded the precursor [**5**]Cl with a single coordinated inhibitor, which maintained a chlorido ligand available for further substitution of a second different inhibitor. Selectivity for the coordination of a single equivalent of inhibitor was achieved in a 20 min reflux reaction in DMF of dichloro(p-cymene)ruthenium(II) dimer, 2 equivalent of B0Cl and 2.2 equivalents H$_2$bapbpy. The coordination of PARP inhibitors Rucaparib and Niraparib to [**5**]Cl were unsuccessful even in the presence of AgPF$_6$, and resulted in a species where the coordinated chlorido ligand was abstracted from the ruthenium and replaced by a solvent molecule (i.e. acetone/methanol/H$_2$O). Even high excess (20 eq.) of the PARP inhibitors did not result in any coordination. This lack of reactivity was attributed to the combined steric hindrance of scaffold [**5**]Cl and the second inhibitor, combined with weakly coordinating groups (pyrrole, amine group). Two inhibitors with stronger pyridine coordinating groups and lower steric hindrance, the NAMPT inhibitor STF31 and the DNA-PK inhibitor PIK75, did bind to [**5**]Cl, yielding compounds [**6**]Cl$_2$ and [**7**]Cl$_2$, respectively. All compounds were fully characterized by NMR, HR-MS and CHN elemental analysis (see Experimental Part).

Single crystals suitable for X-ray structure determination were obtained for three ruthenium conjugates. Interestingly, the acidic crystallization conditions of compounds [**1**]Cl$_2$ and [**3**]Cl$_2$ resulted in the protonation of the N8 and N11 nitrogens of the inhibitors for [**1**+2H]$^{4+}$ and [**3**+2H]$^{4+}$ resulting in tetracationic species. Single crystals of [**1**+2H](Otf)$_4$(THF)$_2$(Et$_2$O) were grown by vapor diffusion of diethylether into a THF solution containing [**1**]Cl$_2$ (0.2 mg/mL) and 2 drops of triflic acid. For [**3**+2H](PF$_6$)$_4$(H$_2$O)$_2$ diethylether diffusion into a methanolic solution of [**3**]Cl$_2$ (0.2 mg/mL) containing a drop of 55% HPF$_6$ in water resulted in single crystals suitable for x-ray diffraction experiments. Lastly, crystals of [**5**]Cl were obtained by vapor diffusion of diethylether into a methanolic solution of [**5**]Cl (0.2 mg/mL) to obtain structure [**5**](Cl)(MeOH)$_2$. The cationic part of the resulting crystal structures are shown in Figure 2 and a selection of bond lengths and angles is reported in table 1. Upon metal coordination, the H$_2$bapbpy

ligand can no longer adopt a flat conformation due to the steric clash between its terminal pyridines, which imposes a helical conformation to the tetrapyridyl structure. We previously reported that the terminal pyridines of the Ru-H$_2$bapbpy scaffold can freely interconvert at room temperature, which is also expected for these compounds.[22] All three compounds showed the presence of both enantiomers in the crystal lattice.

The N1-N3-N4-N6 dihedral angle was calculated as a measure of the distortion of the coordination sphere, with values ranging from 7.1 to 15.5, similar to literature values of other H$_2$bapby-based metal complexes.[22–24] The protonation and the resulting increase in positive charge were not observed for the isolated compounds; it is only a result of the acidic crystallization in the presence of a strong acid. For example, the crystals of [5](Cl)(MeOH)$_2$ were grown in the absence of any acid, and the structure did not show protonation of the B0Cl inhibitor.
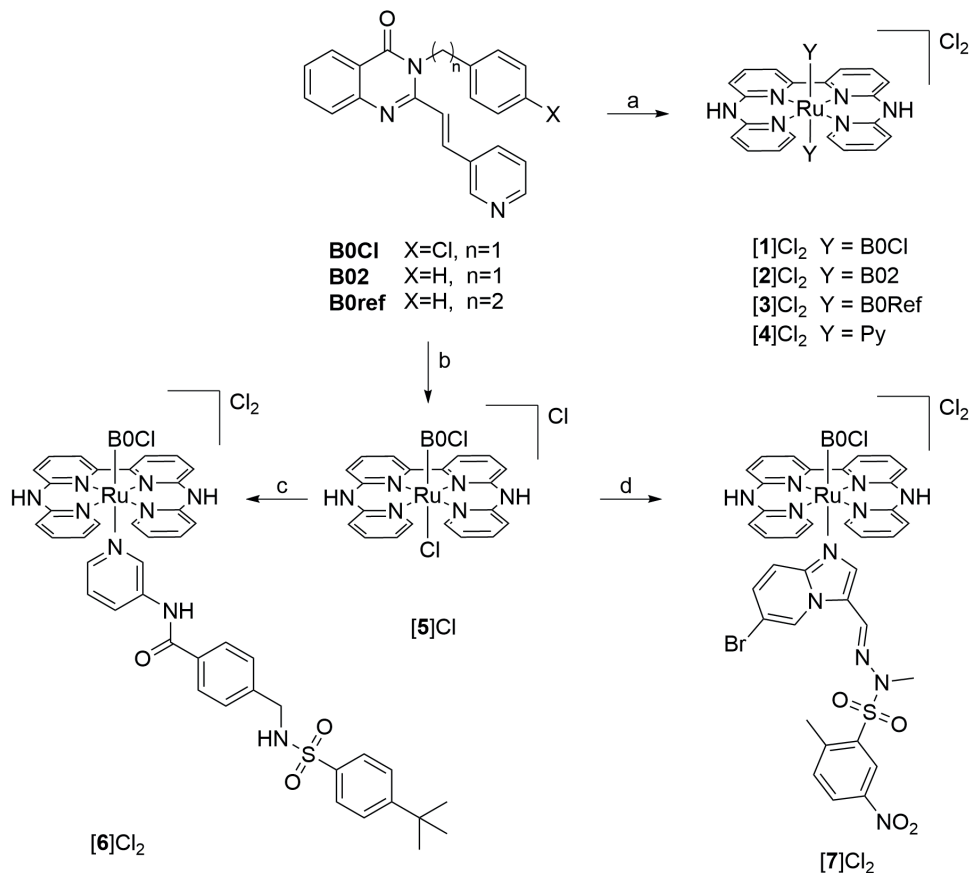

Figure 1. Synthesis of ruthenium compounds [1]Cl$_2$–[7]Cl$_2$. a) Dichloro(p-cymene)ruthenium(II) dimer, H$_2$bapbpy, 2.2 eq., AgPF$_6$ 5 eq., inhibitor 5 eq. were refluxed overnight in acetone, yield 30-54 %. b) Di-chloro(p-cymene)ruthenium(II) dimer, H$_2$bapbpy 2.2 eq., inhibitor 1 eq. were refluxed in DMF for 20 min, yield 62%. c) [5]Cl 1 eq, STF31 0.5 eq., AgPF$_6$ 2.2 eq. were refluxed overnight in acetone, yield 51%. d) [5]Cl 1 eq, PIK75 0.5 eq., AgPF$_6$ 2.2 eq. were refluxed overnight in acetone, yield 51%.
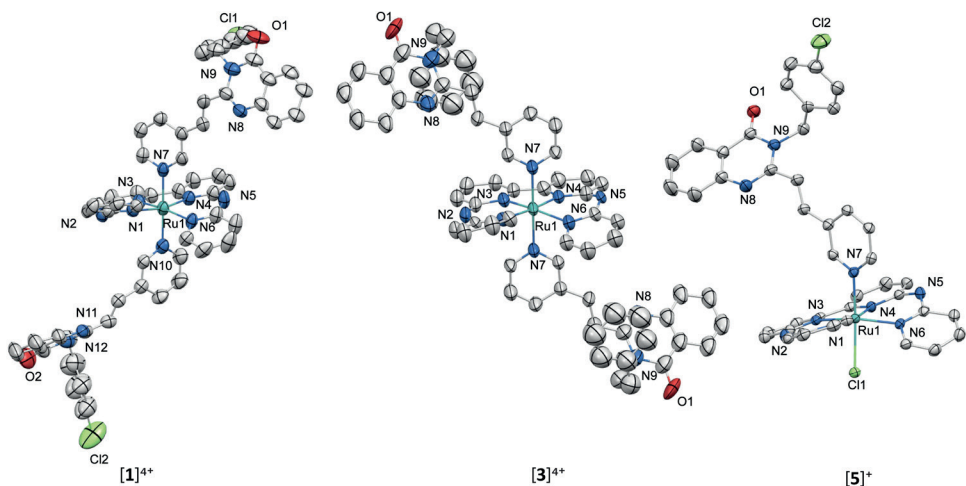
Figure 2 Displacement ellipsoid plots (50% probability level) for [1](Otf)$_4$(THF)$_2$(Et$_2$O), [3](PF$_6$)$_4$(H$_2$O)$_2$, and [5] (Cl)(MeOH)$_2$. Counter ions, solvent molecules and hydrogen atoms have been omitted for clarity.

Table 1. Selected bond distances (Å) and bond angles (°) in the crystal structures of for complexes [1](Otf)$_4$(THF)$_2$(Et$_2$O), [3](PF$_6$)$_4$(H$_2$O)$_2$, and [5](Cl)(MeOH)$_2$.

Compound	[1]$^{4+}$	[3]$^{4+}$	[5]$^+$
M-N1	2.093(4)	2.223(9)	2.076(4)
M-N3	2.026(5)	1.875(6)	2.033(4)
M-N4	2.023(5)	1.915(8)	2.023(4)
M-N6	2.087(5)	2.229(2)	2.088(4)
M-N7	2.119(5)	2.207(2)	2.083(4)
M-N10/Cl1	2.094(5)	-	2.414(1)
C5-N2-C6	132.0(5)	130.7(8)	134.3(4)
C15-N5-C16	133.6(6)	134.4(6)	130.5(4)
N1-M-N4	166.6(2)	175.5(1)	170.1(1)
N3-M-N6	166.9(2)	174.5(2)	165.1(1)
τ$_4$^{a}	0.1(9)	0.0(7)	0.1(8)
Torsion angle N1-N3-N4-N6	15.5(3)	7.1(7)	13.1(6)

^{a} The coordination angles N1-M-N4 (α) and N3-M-N6 (β) were used to calculate. [21]

$$\tau_4 = \frac{360 - (\alpha + \beta)}{141}$$

5.3 Photosubstitution ^{1}H NMR studies

Ruthenium(II) polypyridyl complexes with a distorted first coordination sphere are typically prone to photosubstitution reactions.[25,26] The blue light (435 nm) activation of compounds [1]Cl$_2$, [6]Cl$_2$ and [7]Cl$_2$ in 10/90 MeOH/MeCN was hence monitored by

^{1}H NMR (figures 4-6) and electrospray ionization mass spectrometry (figures SIV.1 – SIV.3). The samples were deoxygenated and irradiated in a blue light photoreactor (450 nm) for 1, 3, 5, 10 and 20 min. ^{1}H-NMR spectra were measured after each irradiation. Light activation of [**1**]Cl$_2$ was observed as a straightforward photosubstitution of one of the two identical inhibitors by a solvent molecule (MeCN) or a chloride counterion. The reaction could easily be monitored by ^{1}H NMR, following the CH$_2$ signal of the B0Cl inhibitor of complex [**1**]Cl$_2$ at 5.4 ppm, (marked with ● in Figure 4). When light irradiation time increased, this signal slowly decreased while the CH$_2$ signal of the free inhibitor at 5.55 ppm gradually appeared (marked with ○ in Figure 4). Interestingly, only two singlet peaks were observed for this CH$_2$ group, i.e., the one for the two coordinated B0Cl molecules in complex [**1**]Cl$_2$, and that of the free inhibitor. The mono-substituted species could not be detected by a separate CH$_2$ peak, probably due to overlap with the CH$_2$ peak of [**1**]Cl$_2$ at 5.4 ppm. Substitution of one inhibitor does probably not lead to significant shift for the CH$_2$ group of the remaining inhibitor. This effect is reasonable, considering the considerable distance between the CH$_2$ group and the metal center. Interestingly, the ESI-MS spectra of the reaction product showed the presence of both [Ru(H$_2$bapbpy)(MeCN)$_2$ – H$^+$]$^+$ at m/z = 523.1 (calc. m/z = 523.2) and of [Ru(H$_2$bapbpy)(MeCN)(Cl)]$^+$ at m/z = 518.0 (calc. m/z = 518.1). The ^{1}H-NMR, however, showed only the formation of one single compound, likely [Ru(H$_2$bapbpy)(MeCN)$_2$]Cl$_2$, suggesting that the chloride-bound species might form during ionization in the mass spectrometer.

The evolution of the ^{1}H NMR spectrum of the dissymmetric complex [**6**]Cl$_2$ containing a B0Cl and a STF31 inhibitor during light activation is shown in Figure 5. The spectra demonstrated the photosubstitution of the two distinct inhibitors by solvent or chloride molecules, which was corroborated by ESI-MS analysis showing peaks for [Ru(H$_2$bapbpy)(MeCN)(Cl)]$^+$ at m/z = 518.0 (calc. 518.1). The reactions could also be followed by the signal of the CH$_2$ group of B0Cl around 5.4 ppm (● coordinated, ○ free inhibitor), as well as the CH$_2$ of STF31 around 4.1 ppm (◆ coordinated, ◇ free inhibitor). Both singlets characteristic for the coordinated inhibitors diminished while the two signals of the two free inhibitors emerged. A distinct signal for the monosubstituted compound could also not be seen here. Based on the integrals of the CH$_2$ groups, the B0Cl inhibitor photocleavage occurred at a faster rate than that of STF31, with the caveat that the signal for the coordinated inhibitor in the monosubstituted species overlapped with the starting prodrug [**6**]Cl$_2$ (Figure 3). The deviation in photosubstitution rates is remarkable as both STF31 and B0Cl are coordinated to ruthenium by a pyridine with minimal steric strain, as the backbone of both inhibitors is positioned at the 3-position on the pyridine ring, i.e., away from the metal center. On the other hand, towards the end of the photoreaction (20 min) both integrals became close (0.89 vs. 0.80 eq.), and probably would converge to 100% release upon longer irradiation times.
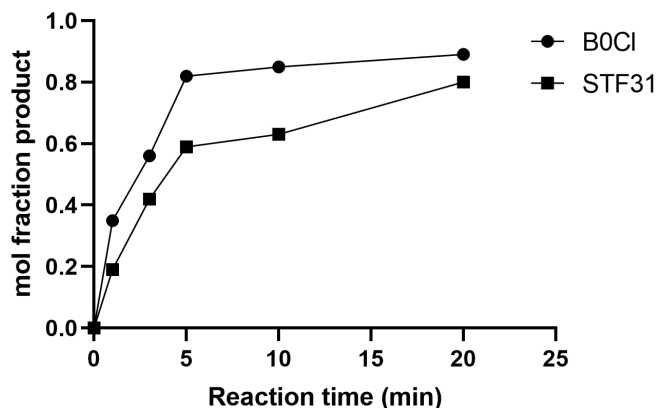
Figure 3. Mol fraction of the photoreleased free inhibitor obtained from the integrals of the CH_2 groups in the ^1H NMR spectrum of a solution of [**6**]Cl_2 irradiated with blue light (435 nm) in 10/90 MeOH/MeCN.
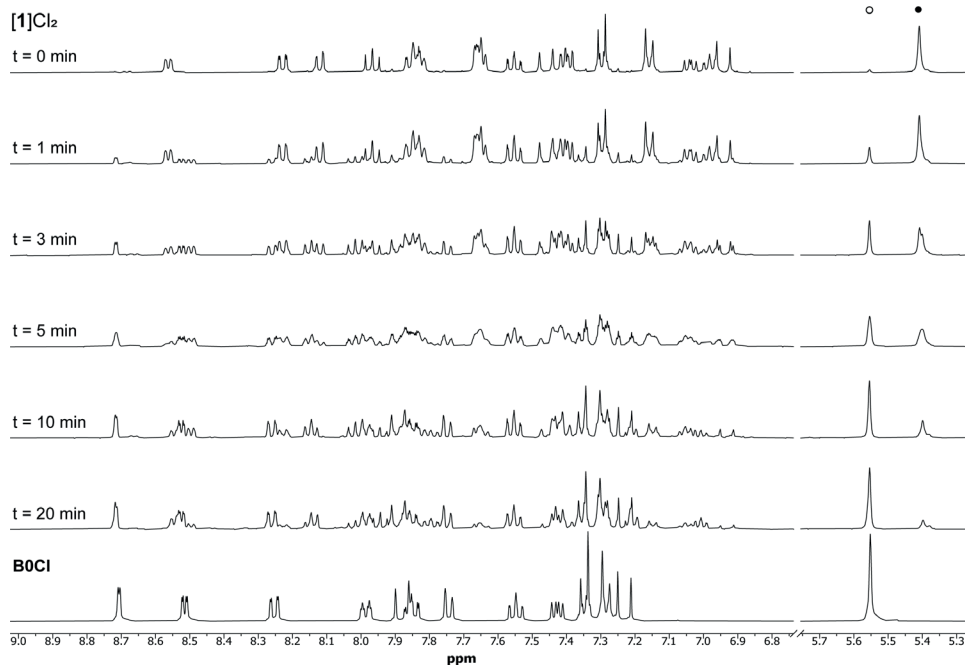
Figure 4. Time evolution of the ^1H NMR spectra of a solution of [**1**]Cl_2 in 10/90 MeOH/MeCN upon irradiation with blue light (450 nm). The CH2 group of B0Cl is indicated at approximately 5.4 ppm (● coordinated, ○ free inhibitor).

The photosubstitution of the second dissymmetric photocaged compound [**7**]Cl_2, which was monitored vs. irradiation time by ^1H NMR, is shown in Figure 6. The spectra evolved in a similar fashion compared with [**6**]Cl_2, notably regarding the CH_2 signal of B0Cl around
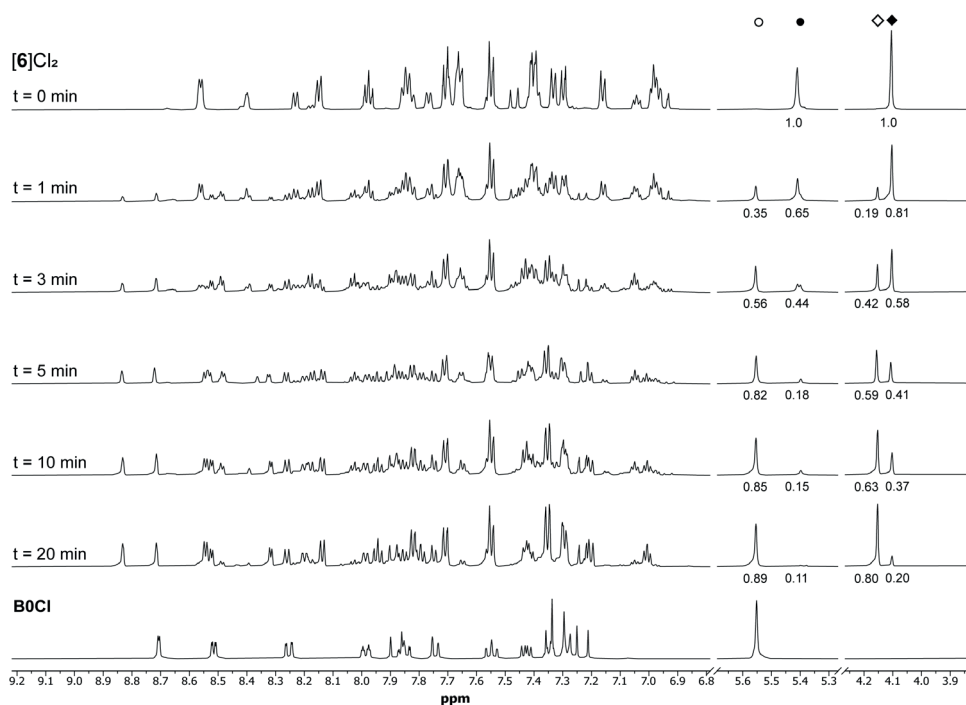
Figure 5. Time evolution of the ^{1}H-NMR spectra of [**6**]Cl$_2$ in 10/90 MeOH/MeCN irradiated with blue light (450 nm). Integrals of a selection of aliphatic peaks are given below the x axis. The CH2 group of B0Cl is indicated at approximately 5.4 ppm (● coordinated, ○ free inhibitor), as well as the CH$_2$ of STF31 around 4.1 ppm (◆ coordinated, ◇ free inhibitor).

5.4 ppm, which went from fully coordinated at the start of the reaction to completely free after 20 min (● coordinated, ○ free inhibitor). The doublet around 6.5 ppm was attributed to the aromatic ring fused to the coordinating imidazole (◆ coordinated) of the PIK75 inhibitor; it slowly disappeared when irradiation time increased, but for this compound two steps could be identified. The first step was characterized by a small upfield shift (0.05 ppm), while the second step was accompanied by a larger upfield shift. The first shift was attributed to photosubstitution of B0Cl, thus keeping the PIK75 inhibitor bound. The ◆ signal showed increased sensitivity towards the changes in environment induced by the photosubstitution of the B0Cl inhibitor, notably in comparison with [**1**]Cl$_2$ or [**6**]Cl$_2$. This effect was attributed to the fact that the hydrogen is part of the aromatic pyridine-imidazole ligand directly coordinated to ruthenium, which is more sensitive to changes of the coordination sphere occurring in *trans* position of the metal center. Overall, all double photocaged inhibitors showed straightforward photosubstitution of both inhibitors with solvent molecules within a reasonable time frame, demonstrating that local activation of a single ruthenium compound could release two distinct inhibitors.
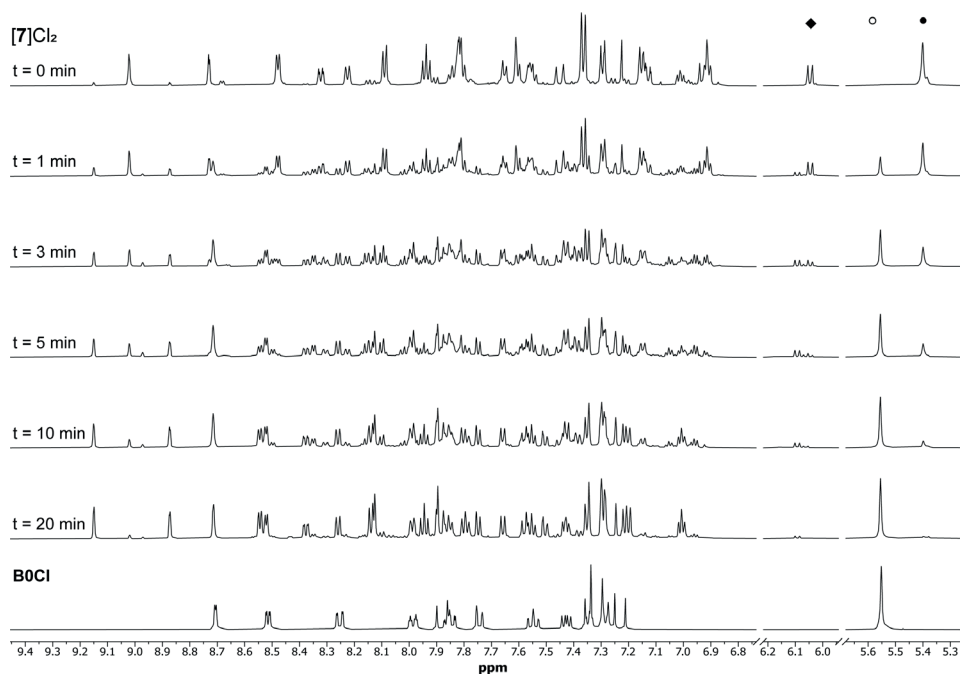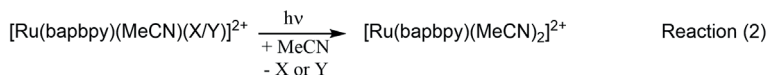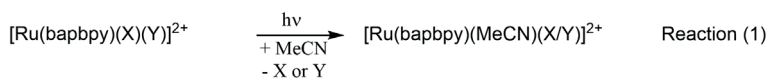
Figure 6. ^{1}H-NMR time evolution spectra of [**7**]Cl$_2$ in 10/90 MeOH/MeCN and irradiated with blue light 450 nm. The CH2 group of B0Cl is indicated at approximately 5.4 ppm (● coordinated, ○ free inhibitor), as well as an aromatic hydrogen located in proximity to the coordinating group of PIK75 around 4.1 ppm (◆ coordinated).

5.4 Photosubstitution quantum yields

The molecular extinction coefficients of the ruthenium H$_2$bapbpy complexes bearing two inhibitors are very similar (Figure 7). The absorption spectra showed peaks or plateaus around 475 nm and ε values between $4 \cdot 10^3$ M^{-1}cm^{-1} and $6 \cdot 10^3$ M^{-1}cm^{-1}. Especially the absorbance of compounds [**1**]Cl$_2$–[**3**]Cl$_2$ was almost identical as the small changes to the molecular formulae of the inhibitors poorly affects the electronic properties of the ruthenium complexes. Photosubstitution quantum yields were determined by 435 nm blue light irradiation in a 10/90 MeOH/MeCN solution of each complex while following in time the UV-Vis spectrum of the solution. Figure 7b shows the time evolution of the UV-Vis spectrum of [**1**]Cl$_2$ and of the absorbance at 505 nm (inset). The spectra clearly show two distinct steps without isosbestic points, which is in accordance with the non-selective photosubstitution of both B0Cl inhibitors. The collected UV-vis data was globally fitted via a method described in the literature utilizing the Glotaran software[27] to determine concentration profiles for the starting, intermediate, and final compounds.[28] The first quantum yield of photosubstitution for reaction 1 (φ_{s1}), and the second for reaction 2 (φ_{s2}), were calculated from the globally fitted data according to a literature procedure and are reported in Table 2.[29] The concentration profiles and calculated quantum yields for [**1**]Cl$_2$ are shown in figure 7, while the other compounds are shown in figures SIV.4-SIV-8.

136

$$[\text{Ru(bapbpy)(X)(Y)}]^{2+} \xrightarrow[\substack{+\text{ MeCN} \\ -\text{ X or Y}}]{h\nu} [\text{Ru(bapbpy)(MeCN)(X/Y)}]^{2+} \qquad \text{Reaction (1)}$$

$$[\text{Ru(bapbpy)(MeCN)(X/Y)}]^{2+} \xrightarrow[\substack{+\text{ MeCN} \\ -\text{ X or Y}}]{h\nu} [\text{Ru(bapbpy)(MeCN)}_2]^{2+} \qquad \text{Reaction (2)}$$

Compounds [1]Cl$_2$–[3]Cl$_2$ exhibited similar photochemical properties with φ_{s1} around 0.05 and significantly lower quantum yield φ_{s2} values around 0.003. The photosubstitution quantum yields of compound [4]Cl$_2$ were in the same order of magnitude as for [1]Cl$_2$–[3]Cl$_2$ as the pyridines are not significantly different from the RAD51 inhibitors. Compounds [6]Cl$_2$ and [7]Cl$_2$ are slightly more intriguing as two light reactions can be considered as first step, with 2 distinct monosubstituted intermediates resulting from the photosubstitution of B0Cl or STF31/PIK75, respectively. However, independently from the detail of the first photosubstituted ligand the main contribution to the observed change in absorption spectrum results from the substitution of a pyridine-based group with a MeCN solvent molecule. The difference in absorbance between the different pyridines-based inhibitors was minimal, which allowed the assumption that both intermediates had similar absorption spectra so that they could be modeled in Glotaran as one single moiety. The resulting photosubstitution quantum yields for compounds [6]Cl$_2$ and [7]Cl$_2$ were similar to the ones for the other ruthenium complexes and the spectra are shown figures SIV.7 and SIV.8. In general, all compounds showed double substitution reaction and shared similar quantum yields as all compounds have the same ruthenium H$_2$bapbpy backbone with two monodentate pyridines-based moieties coordinated in axial position.
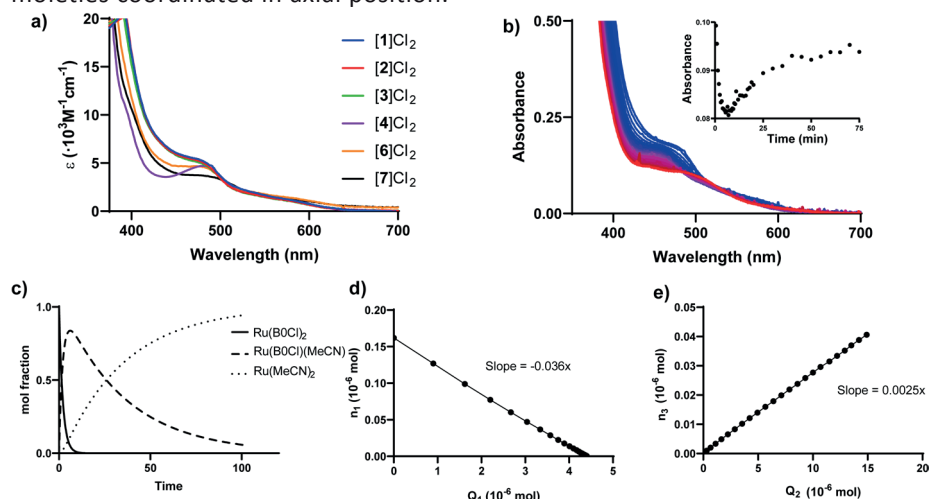
Figure 7 a) UV-Vis spectra plotted as molar extinction coefficients of [1]Cl$_2$-[7]Cl$_2$. b) Time evolution spectra of [1]Cl$_2$ upon blue light irradiation (435 nm), inlay the absorbance at 505 nm. c) Reaction profile calculated by Glotaran for [1]Cl$_2$. d) Amount of Ru(B0Cl)$_2$ (n_1) in mol vs absorbed photons by Ru(B0Cl)$_2$ (Q_1) in mol, where the slope is the quantum yield of the first substitution reaction of [1]Cl$_2$. e) Amount of Ru(MeCN)$_2$ (n_3) in mol vs absorbed photons by Ru(B0Cl)(MeCN) (Q_2) in mol, where the slope is the quantum yield of the second substitution reaction of [1]Cl$_2$.

Table 2. Photosubstitution quantum yields for ruthenium compounds [1]Cl$_2$-[7]Cl$_2$.

Compound	φ_{s1}	φ_{s2}
[1]Cl$_2$	0.036	0.0025
[2]Cl$_2$	0.058	0.0022
[3]Cl$_2$	0.052	0.0025
[4]Cl$_2$	0.099	0.0035
[6]Cl$_2$	0.061	0.0027
[7]Cl$_2$	0.071	0.0027

5.5 Conclusion

In this work we described the synthesis of seven novel ruthenium compounds based on the [Ru(H$_2$bapbpy)(X)(Y)]Cl$_2$ scaffold axially coordinating two pyridine-based ligand X and Y. Ruthenium compounds [1]Cl$_2$–[3]Cl$_2$ bore 2 identical RAD51-based inhibitors while compound [4]Cl$_2$ had two simple pyridine ligands and can be used as a control compound. The coordination of a single B0Cl inhibitor was achieved to form the asymmetric compound [5]Cl with B0Cl on one side and a chlorido ligand coordinated in *trans* fashion. The chlorido ligand was subsequently abstracted to synthesize dissymmetric compound [6]Cl$_2$ and [7]Cl$_2$ bearing two distinct inhibitors: B0Cl and STF31 for [6]Cl$_2$ and B0Cl and PIK75 for [7]Cl$_2$. ^{1}H-NMR blue light irradiation experiments combined with MS analysis demonstrated the successful light-induced uncaging of the two inhibitors while the compounds remained inert in the dark. The quantum yields of photosubstitution upon blue light (435 nm) irradiation were ~0.06 for the first step and ~0.003 for the second one. In conclusion, we demonstrated the possibility to use the ruthenium H$_2$bapbpy scaffold for the photocaging of two distinct inhibitors on a single ruthenium fragment. *In vitro* studies are currently ongoing to study the biological properties of these complexes in cancer cells.

5.6 Experimental
5.6.1 General

All commercially available reagents were bought from Sigma-Aldrich and used as received. PIK75 hydrochloride was bought from medchemexpress. STF31 was synthesized according literature procedures.[30] Inhibitors B0Cl, B02, B0Ref were synthesized as described in chapter 4, and H$_2$bapbpy as described in chapter 2. Filters used were Whatman® regenerated cellulose membrane filters, RC60 Membrane Circles, diam. 47 mm, pore size 1 μm. NMR spectra were recorded on a Bruker, AV-300, AV-400, AV-500, AV-600, or AV-850 spectrometers. High resolution mass spectra (HRMS) were recorded on Waters XEVO-G2 XSQ-TOF) mass spectrometer equipped with an electrospray ion source in positive mode (source voltage 3.0 kV, desolvation gas flow 900 L/hr, temperature 250 °C) with resolution R= 22000 (mass range m/z = 50-2000)

and 200 pg/uL Leu-enkephalin (m/z = 556.2771) as a "lock mass".

5.6.2 Photochemistry

Substitution quantum yields were determined on an Agilent Technologies Cary 60 UV-vis spectrometer. A 0.3 mL aliquot of the stock solution of the ruthenium complex was added to a cuvette containing 2.70 mL MeCN for a final concentration of ~10^{-5}M). The solution was deoxygenated by bubbling N$_2$ for 5 min while stirring with a magnetic bar. The solution was then radiated from above with a 435 nm monochromatic LED. The photon flux in such conditions was determined by ferrioxalate actinometry.[32] Both the cuvette and the LED were temperature controlled at 25 °C. Concentration profiles were globally fitted using the Glotaran software and photosubstitution quantum yields were then determined by the two-wavelength method described in the literature.[33] Dark controls were measured in a similar method but without irradiation.

5.6.3 Synthesis

5.6.3.1 [Ru(H$_2$bapbpy)(B0Cl)$_2$]Cl$_2$ ([1]Cl$_2$)

A solution of dichloro(p-cymene)ruthenium(II) dimer (100 mg, 0.16 mmol), H$_2$bapbpy (116 mg, 0.34 mmol 2,2 eq.), B0Cl (268 mg, 0.72 mmol, 5 eq., and AgPF$_6$ (181 mg, 0.71 mmol, 5 eq.) in deoxygenated acetone (50 mL) was refluxed overnight under nitrogen. The solution was filtered hot over Celite® and washed with acetone (20 mL). The filtrate was concentrated and dissolved in a minimal amount of acetone (5 mL) to which EtOAc (5 mL) was added. Saturated tetraethylammonium chloride in EtOAc was added (2 mL) and the red/brownish precipitate was filtered, washed with EtOAc (40 mL), diethylether (2 x 40 mL) and dried in vacuo to afford the title compound. Yield: 120 mg, 0.09 mmol, 30 %. Rf = 0.8 in acetone:Sat.aq.KPF 9:1. **^{1}H NMR** (500 MHz, DMSO) δ 12.15 (s, 1H), 8.67 (d, J = 6.2 Hz, 1H), 8.34 (d, J = 7.9 Hz, 1H), 8.17 (dd, J = 8.0, 1.0 Hz, 0H), 8.08 (d, J = 8.2 Hz, 0H), 8.03 (t, J = 8.0 Hz, 1H), 7.96 (d, J = 1.8 Hz, 1H), 7.92 − 7.82 (m, 2H), 7.75 (t, J = 8.2 Hz, 1H), 7.70 (d, J = 7.9 Hz, 0H), 7.61 − 7.52 (m, 2H), 7.47 (d, J = 5.7 Hz, 1H), 7.37 − 7.30 (m, 2H), 7.25 − 7.18 (m, 3H), 7.14 (dd, J = 8.1, 5.7 Hz, 1H), 7.03 (t, J = 6.7 Hz, 1H), 5.51 (s, 2H). **^{13}C NMR** (126 MHz, DMSO) δ 161.82 (Cq), 155.56 (Cq), 153.41 (CH), 153.00 (CH), 152.58 (CH), 151.79 (Cq), 151.60 (Cq), 147.34 (Cq), 137.94 (CH) 137.10 (CH), 136.52 (Cq), 135.39 (CH), 134.77 (CH), 133.21 (Cq), 132.45 (Cq), 129.21 (CH), 129.02 (CH), 127.73 (CH), 127.66 (CH), 127.18 (CH), 126.05 (CH), 124.11 (CH), 120.65 (Cq), 115.96 (CH), 45.43 (CH$_2$). **HR-MS** [M-2Cl]$^{2+}$: 594.12219 (calculated); 594.12175 (measured). **Elem. Anal. Calc.** for [C$_{64}$H$_{48}$Cl$_4$N$_{12}$O$_2$Ru]: C 61.01, H 3.84, N 13.34. Found: C 60.73, H 3.84, N 13.24.

5.6.3.2 [Ru(H$_2$bapbpy)(B02)$_2$]Cl$_2$ ([2]Cl$_2$)

Compound [2]Cl$_2$ was synthesized according the procedure described for [1]Cl$_2$ starting

from dichloro(p-cymene)ruthenium(II) dimer (0.16 mmol scale) but with B02 (0.70 mmol) instead of B0Cl to afford the title compound as a red brown solid. Yield 149 mg, 0.12 mmol, 39 %. Rf = 0.8 in acetone:Sat.aq.KPF 9:1. **^{1}H NMR** (500 MHz, DMSO) δ 12.25 (s, 1H), 8.65 (d, J = 6.2 Hz, 1H), 8.31 (d, J = 7.8 Hz, 1H), 8.20 – 8.14 (m, 1H), 8.06 – 7.98 (m, 2H), 7.94 – 7.82 (m, 3H), 7.79 (t, J = 8.4 Hz, 2H), 7.70 (dt, J = 8.1, 0.9 Hz, 1H), 7.60 – 7.50 (m, 2H), 7.48 (d, J = 5.7 Hz, 1H), 7.31 – 7.18 (m, 4H), 7.17 – 7.10 (m, 3H), 7.03 (t, J = 6.4 Hz, 1H), 5.53 (s, 2H). **^{13}C NMR** (126 MHz, DMSO) δ 161.21 (Cq), 154.89 (Cq), 152.54 (CH), 152.35 (CH), 152.15 (CH), 151.98 (Cq), 151.29 (Cq), 150.98 (Cq), 146.72 (Cq), 137.41 (CH), 136.88 (Cq), 136.61 (CH), 134.72 (CH), 134.47 (CH), 134.16 (CH), 132.62 (Cq), 128.63 (CH), 127.29 (CH), 127.10 (CH), 127.00 (CH), 126.56 (CH), 126.40 (CH), 125.43 (CH), 123.72 (CH), 120.03 (Cq), 118.39 (CH), 117.85 (CH), 115.37 (CH), 113.90 (CH), 45.31 (CH$_2$). **HR-MS** [M-2Cl]$^{2+}$: 560.16147 (calculated); 560.16161 (measured). **Elem. Anal. Calc.** for [C$_{64}$H$_{50}$Cl$_2$N$_{12}$O$_2$Ru]: C 64.53, H 4.23, N 14.11. Found: C 63.40, H 4.19, N 13.84.

5.6.3.3 [Ru(H$_2$bapbpy)(B0Ref)$_2$]Cl$_2$ ([3]Cl$_2$)

Compound [**3**]Cl$_2$ was synthesized according the procedure described for [**1**]Cl$_2$ starting from dichloro(p-cymene)ruthenium(II) dimer (0.16 mmol scale) but with B0Ref (0.76 mmol) instead of B0Cl to afford the title compound as a red brown solid. Yield 211 mg, 0.17 mmol, 54 %. Rf = 0.8 in acetone:Sat.aq.KPF 9:1. **^{1}H NMR** (500 MHz, DMSO) δ 12.31 (s, 1H), 8.73 (d, J = 4.6 Hz, 0H), 8.45 (d, J = 7.0 Hz, 1H), 8.13 (dd, J = 8.0, 1.6 Hz, 2H), 8.08 (t, J = 8.0 Hz, 1H), 7.97 – 7.89 (m, 2H), 7.85 (d, J = 8.3 Hz, 2H), 7.81 (ddd, J = 8.5, 7.1, 1.6 Hz, 1H), 7.64 (d, J = 8.0 Hz, 1H), 7.55 – 7.49 (m, 1H), 7.29 (d, J = 15.4 Hz, 1H), 7.20 (dd, J = 8.1, 5.7 Hz, 1H), 7.13 – 7.05 (m, 2H), 7.05 (t, J = 2.0 Hz, 2H), 7.05 – 6.99 (m, 2H), 6.98 – 6.91 (m, 1H), 4.44 (t, J = 7.1 Hz, 2H), 2.91 (t, J = 7.0 Hz, 2H). **^{13}C NMR** (126 MHz, DMSO) δ 161.48 (Cq), 155.63 (Cq), 153.08 (CH), 152.90 (CH), 152.78 (CH), 152.67 (Cq), 152.03 (Cq), 151.64 (Cq), 147.27 (Cq), 138.57 (CH), 138.12 (CH), 137.32 (CH), 135.08 (CH), 134.99 (CH), 134.21 (CH), 133.53 (Cq), 129.49 (CH), 128.79 (CH), 127.60 (CH), 127.35 (CH), 126.98 (CH), 126.93 (CH), 125.99 (CH), 124.22 (CH), 120.62 (Cq), 119.06 (CH), 118.55 (CH), 116.00 (CH), 115.02 (CH), 44.79(CH$_2$), 34.70 (CH$_2$). **HR-MS** [M-2Cl]$^{2+}$: 574.17715 (calculated); 574.17733 (measured). **Elem. Anal. Calc.** for [C$_{66}$H$_{54}$Cl$_2$N$_{12}$O$_2$Ru]: C 65.02, H 4.46, N 13.79. Found: C 64.81, H 4.51, N 13.69.

5.6.3.4 [Ru(H$_2$bapbpy)(Py)$_2$]Cl$_2$ ([4]Cl$_2$)

A solution of dichloro(p-cymene)ruthenium(II) dimer (152 mg, 0.25 mmol), H$_2$bapbpy (177 mg, 0.52 mmol), pyridine (0.5 mL) and AgPF$_6$ (276 mg, 1.09 mmol) in deoxygenated acetone (50 mL) was refluxed overnight under nitrogen. The solution was filtered hot over Celite® and washed with acetone (20 mL). The filtrate was concentrated and dissolved in a minimal amount of acetone (5 mL) to which EtOAc (5 mL) was added. Saturated tetraethylammonium chloride in EtOAc was added (2 mL) and the red/brownish

precipitate was filtered, washed with EtOAc (40 mL), diethylether (2 x 40 mL) and dried in vacuo to afford the title compound. Yield: 139 mg, 0.21 mmol, 42 %. Rf = 0.8 in acetone:Sat.aq.KPF 9:1. **^{1}H NMR** (600 MHz, MeOD) δ 8.62 (d, J = 4.5 Hz, 0H), 8.29 (d, J = 7.7 Hz, 1H), 8.00 (t, J = 8.0 Hz, 1H), 7.86 (t, J = 7.0 Hz, 1H), 7.74 (d, J = 5.1 Hz, 2H), 7.62 (t, J = 7.7 Hz, 1H), 7.51 (d, J = 8.4 Hz, 2H), 7.07 (t, J = 7.1 Hz, 2H), 7.02 (t, J = 6.0 Hz, 1H). **^{13}C NMR** (151 MHz, MeOD) δ 154.90 (Cq), 151.77 (CH), 151.60 (Cq), 151.26 (CH), 150.44 (Cq), 137.00 (CH), 136.55 (CH), 136.15 (CH), 124.77 (CH), 117.82 (CH), 117.24 (CH), 114.62 (CH), 113.39 (CH). **HR-MS** [M-2Cl]$^{2+}$: 300.06566 (calculated); 300.06551 (measured). **Elem. Anal. Calc.** for [$C_{30}H_{26}Cl_2N_8Ru$]: C 53.74, H 3.91, N 16.71. Found: C 52.91, H 3.99, N 16.55.

5.6.3.5 [Ru(H$_2$bapbpy)(B0Cl)(Cl]Cl ([5]Cl$_2$)

A solution of dichloro(p-cymene)ruthenium(II) dimer (100 mg, 0.16 mmol), H$_2$bapbpy (116 mg, 0.34 mmol), B0Cl (122 mg, 0.33 mmol) in deoxygenated DMF (10 mL) was refluxed for 20 min under nitrogen. The solution was filtered hot and the filtrate was precipitated by the addition of diethylether (50 mL), filtered, washed with dietheylether (50 mL) and dried. The compound was purified over silica column (DCM:MeOH 100:0 → 90:10). The first fraction was collected (Rf = 0.6 in acetone:Sat.aq.KPF 9:1) and dried in vacuo to afford the title compound as a dark red solid. Yield 88 mg, 0.10 mmol, 62 % yield.**^{1}H NMR** (500 MHz, MeOD) δ 8.75 (dd, J = 6.2, 1.7 Hz, 2H), 8.25 − 8.18 (m, 3H), 7.91 (t, J = 8.0 Hz, 2H), 7.88 − 7.75 (m, 4H), 7.73 − 7.64 (m, 3H), 7.54 (ddd, J = 8.2, 7.2, 1.1 Hz, 1H), 7.36 (d, J = 15.5 Hz, 1H), 7.31 (d, J = 7.4 Hz, 1H), 7.27 (d, J = 8.5 Hz, 4H), 7.13 (d, J = 8.5 Hz, 2H), 7.04 − 6.97 (m, 4H), 5.44 (s, 2H). **^{13}C NMR** (214 MHz, DMSO) δ 165.53 (Cq), 161.21 (Cq), 155.23 (Cq), 155.05 (Cq), 152.89 (CH) 152.48 (CH), 151.97 (Cq), 151.82 (CH), 151.17 (Cq), 150.76 (Cq), 146.92 (CH), 146.72 (Cq), 143.49 (CH), 142.12 (Cq), 137.74 (Cq), 137.49 (CH), 136.94 (Cq), 136.73 (CH), 135.90 (Cq), 134.78 (CH), 134.76 (CH), 134.08 (Ch), 132.60 (Cq), 132.28 (Cq), 131.84 (Cq), 128.61 (CH), 128.41 (CH), 127.84 (CH), 127.67 (CH), 127.34 (CH), 127.09 (CH), 127.05 (CH), 126.57 (CH), 126.27 (CH), 125.86 (CH), 125.44 (CH), 125.26 (CH), 123.47 (CH), 120.03 (Cq), 118.36 (CH), 117.91 (CH), 115.39 (CH), 114.29 (CH), 45.62 (CH$_2$), 44.81 (CH$_2$), 30.71 (CH$_3$). **HR-MS** [M-Cl]$^+$: 850.11500 (calculated); 850.11398 (measured). **Elem. Anal. Calc.** for [$C_{42}H_{32}Cl_3N_9ORu$]: C 56.92, H 3.64, N 14.23. Found: C 56.36, H 3.57, N 14.25.

5.6.3.6 [Ru(H$_2$bapbpy)(B0Cl)(STF31]Cl$_2$ ([6]Cl$_2$)

A solution of [**5**]Cl$_2$ (100 mg, 0.25 mmol), STF31 (50 mg, 0.12 mmol) and AgPF$_6$ (113 mg, 0.44 mmol) in deoxygenated acetone (20 mL) was refluxed overnight under nitrogen atmosphere. The solution was filtered hot, rotary evaporated, and purified over silica column (DCM:MeOH 100:0 → 90:10). The desired fraction (Rf = 0.7 in acetone:Sat. aq.KPF 9:1) was concentrated and was dissolved in acetone (15 mL) and was precipitated by the addition of a saturated solution of tetraethylammonium chloride in EtOAc (~ 1

mL) and EtOAc (15 mL). The precipitate was filtered and washed with EtOAc (40 mL), diethyl ether (2 x 40 mL) and dried in vacuo to afford the title compound as a red brown powder. Yield: 74 mg, 0.05 mmol, 51 %. Rf = 0.7 in acetone:Sat.aq.KPF 9:1. **¹H NMR** (850 MHz, DMSO) δ 11.92 (s, 1H), 10.44 (s, 1H), 8.62 (d, J = 6.2 Hz, 2H), 8.49 (s, 1H), 8.39 (d, J = 7.8 Hz, 2H), 8.24 (t, J = 6.4 Hz, 1H), 8.17 (d, J = 6.3 Hz, 0H), 8.08 (d, J = 8.1 Hz, 1H), 8.06 (t, J = 8.0 Hz, 2H), 8.00 (s, 1H), 7.91 (t, J = 7.6 Hz, 2H), 7.89 – 7.85 (m, 1H), 7.71 (d, J = 8.0 Hz, 3H), 7.69 – 7.66 (m, 6H), 7.58 (d, J = 15.7 Hz, 1H), 7.57 – 7.54 (m, 1H), 7.54 (d, J = 8.4 Hz, 2H), 7.49 (d, J = 5.8 Hz, 1H), 7.36 – 7.31 (m, 3H), 7.20 (d, J = 8.5 Hz, 2H), 7.15 (dd, J = 8.0, 5.8 Hz, 1H), 7.10 (dd, J = 8.5, 5.8 Hz, 1H), 7.06 (t, J = 6.6 Hz, 2H), 5.51 (s, 2H), 4.05 (d, J = 6.4 Hz, 2H), 1.26 (s, 9H). **¹³C NMR** (214 MHz, DMSO) δ 165.53 (Cq), 161.21 (Cq), 155.23 (Cq), 155.05 (Cq), 152.89 (CH), 151.70 (Cq), 151.97(CH), 151.17 (Cq), 150.76 (Cq), 146.92 (CH), 146.72 (Cq), 143.49 (CH), 142.12 (Cq), 137.74 (Cq), 137.49 (CH), 136.94 (Cq), 136.73 (CH), 135.90 (Cq), 134.78 (CH), 134.08 (CH), 132.60 (Cq), 132.28 (Cq), 131.84 (Cq), 128.61 (CH), 128.41 (CH), 127.84 (CH), 127.67 (CH), 127.34 (CH), 127.09 (CH), 127.05 (CH), 126.57 (CH), 126.27 (CH), 125.86 (CH), 125.44 (CH), 125.26 (CH), 123.47 (CH), 120.03 (Cq), 118.36 (CH), 117.91 (CH), 115.39 (CH), 114.29 (CH), 45.62 (CH$_2$), 44.81 (CH$_2$), 30.71 (CH$_3$). **ES-MS** [M-2Cl]$^{2+}$: 619.2 (calculated); 619.5 (measured). **HR-MS** [M-2Cl]$^{2+}$: 619.15383 (calculated); 619.15404 (measured). **Elem. Anal. Calc.** for [C$_{65}$H$_{57}$Cl$_3$N$_{12}$O$_4$RuS]: C 59.61, H 4.39, N 12.83. Found: C 58.95, H 4.41, N 12.68.

5.6.3.7 [Ru(H$_2$bapbpy)(B0Cl)(PIK75]Cl$_2$ ([7]Cl$_2$)

A solution of [**5**]Cl$_2$ (100 mg, 0.25 mmol), PIK75 (50 mg, 0.12 mmol) and AgPF$_6$ (101 mg, 0.44 mmol) in deoxygenated acetone (20 mL) was refluxed overnight under nitrogen. The solution was filtered hot, rotary evaporated, and the product was purified over silica column (DCM:MeOH 100:0 → 90:10). The desired fraction (Rf = 0.7 in acetone:Sat. aq.KPF 9:1) was rotary evaporated and was dissolved in acetone (15 mL) and was precipitated by the addition of a saturated solution of tetraethylammonium chloride in EtOAc (~ 1 mL) and EtOAc (15 mL). The precipitate was filtered and washed with EtOAc (40 mL), diethyl ether (2 x 40 mL) and dried in vacuo to afford the title compound as a red brown powder. Yield: 76 mg, 0.05 mmol, 51 %. Rf = 0.7 in acetone:Sat.aq.KPF 9:1. **¹H NMR** (850 MHz, DMSO) δ 11.99 (s, 2H), 8.97 (s, 1H), 8.61 (d, J = 2.5 Hz, 1H), 8.52 (d, J = 6.2 Hz, 2H), 8.41 (dd, J = 8.4, 2.5 Hz, 1H), 8.35 (d, J = 7.6 Hz, 2H), 8.17 (dd, J = 7.9, 1.6 Hz, 1H), 8.09 – 8.01 (m, 4H), 7.97 (s, 1H), 7.87 (dt, J = 13.1, 8.1 Hz, 3H), 7.75 (d, J = 8.4 Hz, 1H), 7.72 – 7.67 (m, 5H), 7.59 (d, J = 15.4 Hz, 1H), 7.56 (t, J = 7.5 Hz, 1H), 7.42 (dd, J = 9.9, 2.0 Hz, 1H), 7.33 (d, J = 8.1 Hz, 2H), 7.24 (s, 1H), 7.23 – 7.17 (m, 3H), 7.11 (t, J = 6.9 Hz, 1H), 6.98 (t, J = 6.5 Hz, 2H), 6.06 (d, J = 10.0 Hz, 1H), 5.50 (s, 2H), 3.35 (s, 3H), 2.59 (s, 3H).
¹³C NMR (214 MHz, DMSO) δ 161.75 (Cq), 155.27 (Cq), 152.76 (CH), 152.14 (CH), 152.10 (Cq) 151.16 (Cq), 150.94 (Cq), 146.71 (Cq), 145.77 (Cq), 145.40 (Cq), 138.83

(CH), 137.54 (CH), 136.67 (CH), 136.56 (Cq), 135.89 (Cq), 134.78 (CH), 134.73 (CH), 134.71 (CH), 133.99 (CH), 133.14 (CH), 132.61 (Cq), 132.22 (CH), 131.84 (Cq), 128.60 (CH), 128.39 (CH), 128.14 (CH), 127.09 (CH), 127.05 (CH), 126.57 (CH), 125.47 (CH), 124.55 (CH), 123.50 (CH), 120.86 (Cq), 120.04 (Cq), 118.42 (CH), 117.92 (CH), 117.00 (CH), 115.25 (CH), 114.26 (CH), 113.89 (CH), 108.30 (Cq), 44.81 (Cq CH_2), 31.46 (Cq CH_3), 19.98 (CH_3). **HR-MS** $[M-2Cl]^{2+}$: 634.07004 (calculated); 634.06955 (measured). **Elem. Anal. Calc.** for $[C_{58}H_{46}Cl_3BrN_{14}O_5RuS]$: C 52.05, H 3.46, N 14.65. Found: C 51.48, H 3.45, N 14.42.

5.7 Literature

(1) Bridges, C. B. The Origin of Variations in Sexual and Sex-Limited Characters. *Am. Nat.* **1922**, *56* (642), 51–63.

(2) Nijman, S. M. B. Synthetic Lethality: General Principles, Utility and Detection Using Genetic Screens in Human Cells. *FEBS Lett.* **2011**, *585* (1), 1–6.

(3) Dobzhansky, T. Genetics of Natural Populations. XIII. Recombination and Variability in Populations of Drosophila Pseudoobscura. *Genetics* **1946**, *31* (3), 269.

(4) Bryant, H. E.; Schultz, N.; Thomas, H. D.; Parker, K. M.; Flower, D.; Lopez, E.; Kyle, S.; Meuth, M.; Curtin, N. J.; Helleday, T. Specific Killing of BRCA2-Deficient Tumours with Inhibitors of Poly(ADP-Ribose) Polymerase. *Nature* **2005**, *434* (7035), 913–917.

(5) Farmer, H.; McCabe, N.; Lord, C. J.; Tutt, A. N. J.; Johnson, D. A.; Richardson, T. B.; Santarosa, M.; Dillon, K. J.; Hickson, I.; Knights, C.; Martin, N. M. B.; Jackson, S. P.; Smith, G. C. M.; Ashworth, A. Targeting the DNA Repair Defect in BRCA Mutant Cells as a Therapeutic Strategy. *Nature* **2005**, *434* (7035), 917–921.

(6) Menezes, M. C.; Raheem, F.; Mina, L.; Ernst, B.; Batalini, F. PARP Inhibitors for Breast Cancer: Germline BRCA1/2 and Beyond. *Cancers* **2022**, *14* (17).

(7) Sunada, S.; Nakanishi, A.; Miki, Y. Crosstalk of DNA Double-Strand Break Repair Pathways in Poly(ADP-Ribose) Polymerase Inhibitor Treatment of Breast Cancer Susceptibility Gene 1/2-Mutated Cancer. *Cancer Sci.* **2018**, *109* (4), 893–899.

(8) Rose, M.; Burgess, J. T.; O'Byrne, K.; Richard, D. J.; Bolderson, E. PARP Inhibitors: Clinical Relevance, Mechanisms of Action and Tumor Resistance. *Front. Cell Dev. Biol.* **2020**, *8*.

(9) Zheng, F.; Zhang, Y.; Chen, S.; Weng, X.; Rao, Y.; Fang, H. Mechanism and Current Progress of Poly ADP-Ribose Polymerase (PARP) Inhibitors in the Treatment of Ovarian Cancer. *Biomed. Pharmacother.* **2020**, *123*, 109661.

(10) Ryan, C. J.; Bajrami, I.; Lord, C. J. Synthetic Lethality and Cancer – Penetrance as the Major Barrier. *Trends Cancer* **2018**, *4* (10), 671–683.

(11) Ashworth, A.; Lord, C. J.; Reis-Filho, J. S. Genetic Interactions in Cancer Progression and Treatment. *Cell* **2011**, *145* (1), 30–38.

(12) Wiegmans, A. P.; Miranda, M.; Wen, S. W.; Al-Ejeh, F.; Möller, A. RAD51 Inhibition in Triple Negative Breast Cancer Cells Is Challenged by Compensatory Survival Signaling and Requires Rational Combination Therapy. *Oncotarget* **2016**, *7* (37), 60087.

(13) Liu, Y.; Burness, M. L.; Martin-Trevino, R.; Guy, J.; Bai, S.; Harouaka, R.; Brooks, M. D.; Shang, L.; Fox, A.; Luther, T. K.; Davis, A.; Baker, T. L.; Colacino, J.; Clouthier, S. G.; Shao, Z.; Wicha, M. S.; Liu, S. RAD51 Mediates Resistance of Cancer Stem Cells to PARP Inhibition in Triple-Negative Breast Cancer. *Clin. Cancer Res.* **2017**, *23* (2), 514–522.

(14) Alagpulinsa, D. A.; Ayyadevara, S.; Shmookler Reis, R. J. A Small-Molecule Inhibitor of RAD51 Reduces Homologous Recombination and Sensitizes Multiple Myeloma Cells to Doxorubicin. *Front. Oncol.* **2014**, *4*.

(15) Heske, C. M. Beyond Energy Metabolism: Exploiting the Additional Roles of NAMPT for Cancer Therapy. *Front. Oncol.* **2020**, *9*.

(16) Touat, M.; Sourisseau, T.; Dorvault, N.; Chabanon, R. M.; Garrido, M.; Morel, D.; Krastev, D. B.; Bigot, L.; Adam, J.; Frankum, J. R.; Durand, S.; Pontoizeau, C.; Souquère, S.; Kuo, M.-S.; Sauvaigo, S.; Mardakheh, F.; Sarasin, A.; Olaussen, K. A.; Friboulet, L.; Bouillaud, F.; Pierron, G.; Ashworth, A.; Lombès, A.; Lord, C. J.; Soria, J.-C.; Postel-Vinay, S. DNA Repair Deficiency Sensitizes Lung Cancer Cells to NAD+ Biosynthesis Blockade. *J. Clin. Invest.* **2018**, *128* (4), 1671–1687.

(17) Zhu, B.; Deng, X.; Sun, Y.; Bai, L.; Xiahou, Z.; Cong, Y.; Xu, X. Nampt Is Involved in DNA Double-Strand Break Repair. *Chin. J. Cancer* **2012**, *31* (8), 392.

(18) Knight, Z. A.; Gonzalez, B.; Feldman, M. E.; Zunder, E. R.; Goldenberg, D. D.; Williams, O.; Loewith, R.; Stokoe, D.; Balla, A.; Toth, B.; Balla, T.; Weiss, W. A.; Williams, R. L.; Shokat, K. M. A Pharmacological Map of the PI3-K Family Defines a Role for P110α in Insulin Signaling. *Cell* **2006**, *125* (4), 733–747.

(19) Juvekar, A.; Hu, H.; Yadegarynia, S.; Lyssiotis, C. A.; Ullas, S.; Lien, E. C.; Bellinger, G.; Son, J.; Hok, R. C.; Seth, P. Phosphoinositide 3-Kinase Inhibitors Induce DNA Damage through Nucleoside Depletion. *Proc. Natl. Acad. Sci.* **2016**, *113* (30), E4338–E4347.

(20) Fok, J. H. L.; Ramos-Montoya, A.; Vazquez-Chantada, M.; Wijnhoven, P. W. G.; Follia, V.; James, N.; Farrington, P. M.; Karmokar, A.; Willis, S. E.; Cairns, J.; Nikkilä, J.; Beattie, D.; Lamont, G. M.; Finlay, M. R. V.; Wilson, J.; Smith, A.; O'Connor, L. O.; Ling, S.; Fawell, S. E.; O'Connor, M. J.; Hollingsworth, S. J.; Dean, E.; Goldberg, F. W.; Davies, B. R.; Cadogan, E. B. AZD7648 Is a Potent and Selective DNA-PK Inhibitor That Enhances Radiation, Chemotherapy and Olaparib Activity.

Nat. Commun. **2019**, *10* (1), 5065.

(21) Addison, A. W.; Rao, T. N.; Reedijk, J.; van Rijn, J.; Verschoor, G. C. Synthesis, Structure, and Spectroscopic Properties of Copper(II) Compounds Containing Nitrogen–Sulphur Donor Ligands; the Crystal and Molecular Structure of Aqua[1,7-Bis(N-Methylbenzimidazol-2'-Yl)-2,6-Dithiaheptane]Copper(II) Perchlorate. *J. Chem. Soc. Dalton Trans.* **1984**, No. 7, 1349–1356.

(22) van de Griend, C.; van de Vijver, J. J.; Siegler, M. A.; Dame, R. T.; Bonnet, S. Ruthenium-Locked Helical Chirality: A Barrier of Inversion and Formation of an Asymmetric Macrocycle. *Inorg. Chem.* **2022**, *61* (40), 16045–16054.

(23) van Rixel, V. H. S.; Busemann, A.; Wissingh, M. F.; Hopkins, S. L.; Siewert, B.; van de Griend, C.; Siegler, M. A.; Marzo, T.; Papi, F.; Ferraroni, M.; Gratteri, P.; Bazzicalupi, C.; Messori, L.; Bonnet, S. Induction of a Four-Way Junction Structure in the DNA Palindromic Hexanucleotide 5'-d(C-GTACG)-3' by a Mononuclear Platinum Complex. *Angew. Chem. Int. Ed.* **2019**, *58* (28), 9378–9382.

(24) van Rixel, V. H. S.; Siewert, B.; Hopkins, S. L.; Askes, S. H. C.; Busemann, A.; Siegler, M. A.; Bonnet, S. Green Light-Induced Apoptosis in Cancer Cells by a Tetrapyridyl Ruthenium Prodrug Offering Two Trans Coordination Sites. *Chem. Sci.* **2016**, *7* (8), 4922–4929.

(25) Mitchell, D. K.; Sauvage, J.-P. A Topologically Chiral [2]Catenand. *Angew. Chem. Int. Ed. Engl.* **1988**, *27* (7), 930–931.

(26) Bonnet, S.; Collin, J.-P.; Sauvage, J.-P. Light-Induced Geometrical Changes in Acyclic Ruthenium(II) Complexes and Their Ruthena–Macrocyclic Analogues. *Inorg. Chem.* **2007**, *46* (25), 10520–10533.

(27) Snellenburg, J. J.; Laptenok, S.; Seger, R.; Mullen, K. M.; van Stokkum, I. H. Glotaran: A Java-Based Graphical User Interface for the R Package TIMP. *J. Stat. Softw.* **2012**, *49*, 1–22.

(28) Meijer, M. S.; Natile, M. M.; Bonnet, S. 796 Nm Activation of a Photocleavable Ruthenium(II) Complex Conjugated to an Upconverting Nanoparticle through Two Phosphonate Groups. *Inorg. Chem.* **2020**, *59* (20), 14807–14818.

(29) Lameijer, L. N.; van de Griend, C.; Hopkins, S. L.; Volbeda, A.-G.; Askes, S. H. C.; Siegler, M. A.; Bonnet, S. Photochemical Resolution of a Thermally Inert Cyclometalated Ru(Phbpy)(N–N)(Sulfoxide)+ Complex. *J. Am. Chem. Soc.* **2019**, *141* (1), 352–362.

(30) Lameijer, L. N.; Ernst, D.; Hopkins, S. L.; Meijer, M. S.; Askes, S. H.; Le Dévédec, S. E.; Bonnet, S. A Red-light-activated Ruthenium-caged NAMPT Inhibitor Remains Phototoxic in Hypoxic Cancer Cells. *Angew. Chem.* **2017**, *129* (38), 11707–11711.

(31) Zhou, X.-Q.; Busemann, A.; Meijer, M. S.; Siegler, M. A.; Bonnet, S. The Two Isomers of a Cyclometallated Palladium Sensitizer Show Different Photodynamic Properties in Cancer Cells. *Chem. Commun.* **2019**, *55* (32), 4695–4698.

(32) Calvert, J.; Pitts, J. Chemical Actinometer for the Determination of Ultraviolet Light Intensities. *Photo Chem. Wiley Sons N. Y.* **1967**, 780.

(33) Bahreman, A.; Limburg, B.; Siegler, M. A.; Bouwman, E.; Bonnet, S. Spontaneous Formation in the Dark, and Visible Light-Induced Cleavage, of a Ru–S Bond in Water: A Thermodynamic and Kinetic Study. *Inorg. Chem.* **2013**, *52* (16), 9456–9469.

5